Talanta 291 (2025) 127760

Contents lists available at ScienceDirect

Talanta

journal homepage: www.elsevier.com/locate/talanta

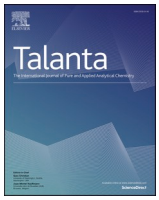

Rapid and sensitive detection of wood smoke exposure biomarkers using europium fluorescent nanoparticle label/lateral flow immunoassay

Yonghao Fu [1], Yang Song [1], Zhansen Yang, Xiaofan Ruan, Yuehe Lin, Dan Du [*]

School of Mechanical and Materials Engineering, Washington State University, Pullman, WA, 99164, USA

ARTICLE INFO

Keywords:
Lateral flow immunoassay
Europium chelates nanoparticles
Wood smoke biomarker
S-phenylmercapturic acid

ABSTRACT

Exposure to wood smoke is associated with various adverse health problems. Biomonitoring of smoke exposure-associated biomarkers provides accurate measurements of personally absorbed doses. As a specific metabolite of benzene, the quantitative measurement of S-phenylmercapturic acid (S-PMA) plays a vital role in evaluating human exposure to wood smoke. In this study, we developed an efficient lateral flow immunoassay (LFIA) approach for accurately and rapidly measuring S-PMA levels. Europium chelate nanoparticles (EuNPs) conjugated with purified polyclonal sheep anti-S-PMA antibodies were employed as the fluorescent detection probe. This work is based on a competitive immunoassay, where the target S-PMA competes with the immobilized antigen on the test lines for the limited antigen-binding sites on EuNP-conjugated antibodies. Due to this competition, the fluorescent intensity of the EuNPs is inversely proportional to the concentration of the target S-PMA in the sample, enabling quantitative measurement. Owing to the large Stokes shift, superior fluorescent brightness, and saturation of the EuNPs, S-PMA levels can be measured with a limit of detection of 0.32 ng/mL, a detectable range of 0.10–30 ng/mL, and a linear detection range of 0.25–30 ng/mL under optimized conditions. Stability testing revealed that the LFIA strips can be stored at room temperature for up to one year while maintaining excellent detection performance for S-PMA. These results demonstrate that the EuNP-based LFIA is a promising tool for accurate preclinical and point-of-care evaluation of wood smoke exposure. A major advantage of this approach is its ability to accurately analyze smoke biomarkers at anticipated low concentrations. The sensor system allows low-cost, rapid, and on-site data collection and quantification of wood smoke exposure.

1. Introduction

In recent years, wildfires have increasingly posed a threat to humans amid climate change [1]. Smoke from these fires has exposed millions to hazardous air quality, sparking global concern [2]. Human exposure to wood smoke is linked to numerous health issues, including respiratory disease, cardiovascular disease, and lung cancer [3–6]. Therefore, accurately measuring this exposure is crucial for both preclinical diagnosis and epidemiological studies. However, effective methods for assessing the exposure levels are lacking due to the chemical complexity and variability of ambient wood smoke [7].

As one of the most extensively studied volatile organic compounds in wildfires and firefighting situations, benzene exhibits genotoxic, immunosuppressive, and carcinogenic properties [8]. Given its rapid metabolism and clearance from the blood, benzene is commonly monitored in urine, either as unmetabolized benzene (u-benzene) or through one of its metabolites [9]. Among these metabolites, S-phenylmercapturic acid (S-PMA) has exhibited the strongest correlation with airborne benzene levels, particularly evident at low benzene levels [10]. The molecular formula of S-PMA is $C_{11}H_{13}NO_3S$, and the process of benzene metabolism in the human body that produces S-PMA is shown in Fig. 1 [11,12]. Besides, previous studies have observed increased benzene levels in the urine of firefighters following exposure to fire emissions, with corresponding increases in S-PMA levels post-firefighting activities [13]. Notably, S-PMA is a specific metabolite of benzene, suggesting that benzene originating from wildfires and urban pollution may contribute to the overall metabolite levels detected in urine [14,15]. Consequently, the monitoring of S-PMA levels in urine provides a viable approach for assessing benzene exposure in wildfire and firefighting scenarios.

Human biomonitoring serves as an essential tool in evaluating individuals' exposure to potentially toxic chemicals, by measuring these

* Corresponding author.
E-mail addresses: yuehe.lin@wsu.edu (Y. Lin), annie.du@wsu.edu (D. Du).
[1] These two authors contributed equally to this work.

https://doi.org/10.1016/j.talanta.2025.127760
Received 23 December 2024; Received in revised form 1 February 2025; Accepted 16 February 2025
Available online 20 February 2025
0039-9140/

substances and their metabolites within the body [16–18]. It provides crucial insights in the diagnosis, treatment, and prevention. Globally, considerable efforts have been invested in establishing biomonitoring programs, reflecting the growing recognition of its significance in public health [19,20]. For monitoring S-PMA, researchers have developed a variety of assays, such as liquid chromatography mass spectrometry (LC-MS) [13], liquid chromatography-tandem mass spectrometry (LC-MS/MS) [21], high-performance liquid chromatography (HPLC) [22], gas chromatography-mass spectrometry (GC-MS) [23], and enzyme-Linked Immunosorbent Assay (ELISA) [24]. Although these classic assays (mainly using chromatographic techniques) offer high accuracy and have been proven effective for personal exposure assessment, their practicality in scenarios such as personal preclinical testing, field evaluation, and large-scale monitoring is limited due to the need for bulky equipment, complex pretreatment, and cost constraints [7,25,26]. However, biosensors are attractive alternatives to address these limitations [27,28]. As analytical devices based on biological recognition of analytes, biosensors with various applications have been used in many fields [28,29]. Among the array of biosensors, immunosensors, which rely on immunochemical reaction for specific analyte detection, have proven particularly influential in food, environmental and disease analyses [30,31]. Recently, with the increasing demand for device miniaturization and diversified application scenarios, the lateral flow immunoassay (LFIA), a type of paper-based immunosensor, has gained prominence owing to its affordability, simplicity, rapid response, and visual readout [32–34]. In our previous studies, LFIA demonstrated accurate detection of multiple targets, including pesticides such as 2, 4-dichlorophenoxyacetic acid [35], atrazine [36], diamino-chlorotriazine [37], acetochlor and fenpropathrin [38], pathogens such as *Salmonella Enteritidis*, *Escherichia coli* O157:H7 [39], as well as biomarkers such as cardiac troponin I-troponin C, and myoglobin [40]. These advantages make LFIA an optimal choice for the point-of-care assessment of S-PMA, while no corresponding application has been reported.

Herein, we present the first application of LFIA for the rapid, quantitative detection of urinary S-PMA as an alternative tool for assessing human exposure to wood smoke. The recognition of S-PMA relied on a competitive immunoassay [41], wherein the sample analyte competed with the coated antigen immobilized on test lines for the limited antigen binding sites on signal reporter, resulting in a signal inversely proportional to the amount of sample analyte. The polyclonal sheep anti-S-PMA antibody was labelled with europium chelate nanoparticle (EuNP), which serves as a signal reporter. The proposed approach offers several key advantages. Firstly, the LFIA approach is simple to operate, quick to respond, making it the best choice for point-of-care testing. At the same time, as a paper-based sensor, its low cost is also a major advantage. Secondly, since LFIA is based on immunochemical reactions, it offers excellent selectivity and specificity. Finally, the EuNP fluorescent label used in the study has the characteristics of large Stokes shift, narrow emission peak and high quantum yield, thus giving the LFIA test strips higher sensitivity and accuracy.

2. Experimental

2.1. Chemicals and materials

BS3 Bis(sulfosuccinimidyl)suberate (BS3), bovine serum albumin (BSA), sodium carbonate buffer, potassium phosphate buffer, phosphate buffered saline (PBS), 2-(N-Morpholino)ethanesulfonic acid (MES), N-Hydroxysuccinimide (NHS), 1-Ethyl-3-(3-dimethylaminopropyl)carbodiimide (EDC), fetal bovine serum (FBS), donkey anti-sheep immunoglobulin G (IgG) polyclonal antibodies, Tris-HCl buffer, Tween-20, nitrocellulose membrane (NC membrane), porous glass fiber were bought from Sigma-Aldrich Chemical Co. (St. Louis, MO). Europium Chelate was bought from Thermo Fisher Scientific Inc. (Waltham, MA). S-PMA ELISA test kit was bought from Chemitrace Consultancy (Natland, United Kingdom).

2.2. Instruments

ÄKTA Fast Protein Liquid Chromatograph (FPLC) System was from Cytiva (Marlborough, MA). Transmission electron microscopes (TEM) images were captured on an FEI Technai G2 20 Twin equipped with a 200 KV LaB6 electron source. Nanodrop 2000 was bought from Thermo Fisher Scientific Inc. (Waltham, MA). Fluorescent immunoanalyzer AFS-1000 was bought from Guangzhou Labsim Biotech Co., Ltd. (Guangzhou, China). BioDot BioJet BJQ 3000 dispenser, BioDot AirJet BJQ 3000 dispenser and BioDot paper cutter module CM4000 were bought from BioDot, Inc. (Irvine, CA, USA). A Safire-II multi-mode microplate reader from Tecan Group Ltd. (Zürich, Switzerland) was used for fluorescence and absorption analysis.

2.3. Synthesis of hapten-BSA conjugate

0.025 mmol of S-phenylcysteine, 0.025 mmol of crosslinker BS3, and 50 mg of BSA were dissolved in 5 mL of sodium carbonate buffer (pH = 9.6). The solution was stirred overnight. Subsequently, the conjugates obtained in this manner were dialyzed against 5 changes of 50 mM potassium phosphate buffer and washed with PBS for 3 days at 4 °C for subsequent use. Then, hapten-BSA conjugate was purified by FPLC. An ultraviolet (UV) detector was used to measure protein concentration at an absorption wavelength of 280 nm.

2.4. Purification of S-PMA polyclonal antibody

Conjugation of hapten-BSA to the resin was performed to develop an S-PMA column for the purification of S-PMA antibody. Subsequently, the S-PMA polyclonal antibody was purified using FPLC and then dialyzed. Protein concentration was measured using a UV detector at an absorption wavelength of 280 nm. The antibody was concentrated in a 50 kDa Centricon tube by centrifugation at 3000*g* for 10 min and filtered through a 0.22 μm filter. The optical density at A280 (OD@A280) of the antibodies, before and after dialysis, was measured using Nanodrop to determine the concentrations of S-PMA antibody.

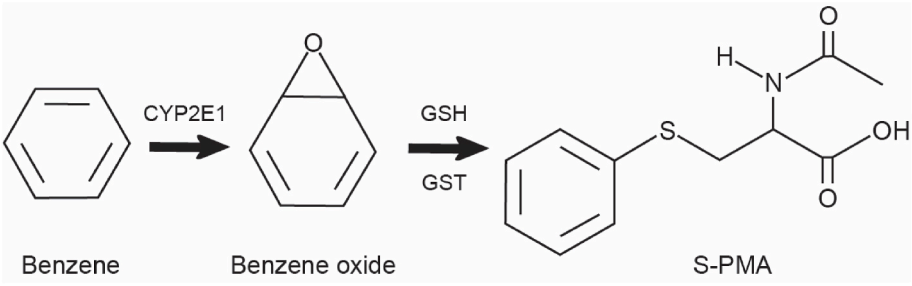

Fig. 1. Metabolism of benzene leading to the production of S-PMA. CYP2E1: Cytochrome P450 2E1. GSH: Glutathione. GST: Glutathione S-transferase.

2.5. Preparation of EuNP-S-PMA antibody conjugate

Purified sheep anti-S-PMA antibody was covalently conjugated to the surface of carboxylate-modified EuNP as follows. First, 20 μL of EuNP (1 % w/v) and 990 μL of MES (50 mM, pH 5.5) were mixed in a 2 mL microcentrifuge tube. Then, 25 μL of 5 mg/mL NHS and 4.8 μL of 5 mg/mL EDC were added and mixed on a rocking shaker at room temperature for 30 min. Next, the solution was centrifuged at 41,657 g for 30 min, the supernatant was removed, and the resulting carboxyl-activated EuNP was resuspended in 1 mL of 10 mM PBS (pH 7.2). Afterwards, sheep anti-S-PMA antibody at a final concentration of 4 μg/mL was added into the above solution and incubated for 1 h at room temperature on a rocking shaker, to conjugate with EuNP. Then 100 μl of FBS was added and incubated for additional 15 min to block the excess binding sites. Finally, the supernatant was removed, and the remaining pellet was washed twice with PBSA (1 % BSA added) and resuspended in 10 % FBS and 10 % sucrose in 0.1 M Tris-HCl buffer (pH 8.2). The final EuNP-antibody conjugate (EuNP-Abs) (approx. 1 μg/mL) was stored at 4 °C before use.

2.6. Preparation for the LFIA test strip

The sample pads (17 mm × 30 cm) composed of glass fiber were saturated with 0.1 M Tris-HCl buffer (pH 8.2) containing 0.25 wt% Tween-20. The pads were then dried at 37 °C for 2 h and stored in the desiccator. Both the test lines and the control line, having the same dispensing rate of 1 μL/cm, were prepared by dispensing hapten-BSA conjugate (1.0 mg/mL) and donkey anti-sheep immunoglobulin G (IgG) polyclonal antibodies (0.5 mg/mL) at different locations on a NC membrane (25 mm × 30 cm) using BioDot BioJet BJQ 3000 dispenser. The NC membranes were then dried at 37 °C for 30 min and stored in a dry room. Subsequently, the conjugate pad (8 mm × 30 cm) was pre-treated with blocking buffer consisting of 0.1 M Tris-HCl with 1 wt% Tween-20, pH 8.2. The conjugation dilution buffer was dispensed onto the conjugate pad using BioDot AirJet BJQ 3000 dispenser. To achieve optimum performance and good repeatability of conjugate pad, the airjet dispenser should be set to a dispensing speed of 15 mm/s with a rate of 1 μL/cm. The dispenser pressure was set to 10 psi. After dispensing, the conjugate pads were then dried at 37 °C for 30 min and stored in dry room for further use. The different pads were assembled on a backing (60 mm × 30 cm) with an overlap of approximately 1–2 mm between them to ensure solution could migrate through the LFIA test strip. The LFIA test strip was cut at a width of 3.5 mm using BioDot paper cutter module CM4000.

2.7. Assay procedure

In a typical assay, the sample was spiked into 200 μL of sample dilution solution (0.05 M Tris-HCl, 0.5 wt% BSA, 0.5 wt% Tween-20) to prepare the spiked buffer. The solution was loaded onto the sample pad of the LFIA test strip. The solution then migrated through the porous glass fiber pads and NC membrane towards the absorbent pad by capillary action. After 15 min, the LFIA test strip was inserted into the lateral flow strips reader, which recorded either the fluorescent intensity or the intensity of test line to the intensity of control line (T/C) ratio.

2.8. Performance evaluation

Serial dilutions of S-PMA were spiked into the sample dilution solution to achieve final concentrations of 0.1, 0.25, 0.5, 1, 1.25, 2.5, 5, 10, 15, 20, and 30 ng/mL in the spiked buffer. The sample solution was also used as the blank. In a typical test, 200 μL of sample dilution solution containing various concentrations of S-PMA was loaded onto the sample pad of LFIA test strip. The solution then migrated through the porous glass fiber pads and NC membrane towards the absorbent pad by capillary action. After 15 min, the LFIA test strip was inserted into the lateral flow strips reader, which recorded either the intensity or the T/C ratio. Additionally, standard curves were generated based on T/C ratio and S-PMA concentrations.

2.9. Stability test

The stability test was performed according to the method of Song et al. [40], with slight modifications. In the stability test, the stability of the LFIA is demonstrated through aging experiments. Briefly, to accelerate aging study, the strip was stored in a sealed plastic bag which was filled with silica bead desiccant at 50 °C. The aging experiment lasted for nine weeks, and the T/C ratios of the samples and the recoveries of urine and serum samples were recorded weekly.

3. Results and discussion

3.1. Detection mechanism

The LFIA for S-PMA analysis employs a competitive format (Fig. 2). The hapten-BSA conjugate serves as the capture antigen on the test line, while donkey anti-sheep IgG polyclonal antibodies are utilized as the secondary antibodies on the control line of LFIA strips. Before the test, capture antibody conjugates (purified sheep anti-S-PMA labelled with EuNP, noted as Eu) were preloaded onto the conjugate pad. In the absence of S-PMA in the running buffer, the sample migrates towards the absorbent pad through capillary action, carrying EuNP-antibody conjugates. These conjugates bind to the capture antigen on the test line, generating a strong fluorescent signal. Any surplus EuNP-antibody conjugates bind to the secondary antibody on the control line. However, in the presence of S-PMA, it competes with hapten-BSA conjugate on the test line for binding to the EuNP-antibody conjugates. This competition inhibits the binding of EuNP-antibody conjugates to the test line, resulting in reduced signal intensity. Consequently, the signal inhibition on the test line is indicative of S-PMA presence. In other words, the measured fluorescent signal strength is inversely proportional to the concentration of S-PMA.

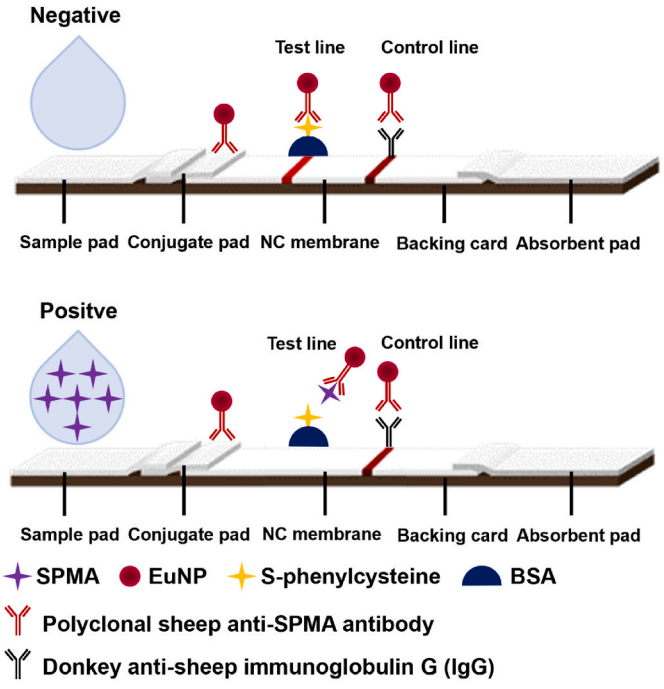

Fig. 2. The detection mechanism of LFIA for S-PMA.

3.2. Synthesis of hapten-BSA conjugate

Fig. 3 illustrates the FPLC chromatogram of hapten-BSA conjugate after FPLC superdex purification. The narrow peak located at around 50 mL indicates the highly purified fraction of hapten-BSA conjugate, while the broader peak at 75 mL corresponds to the unreactive component.

3.3. Purification of S-PMA antibody

Fig. 4 presents the FPLC curve of S-PMA antibody, with the peak at 100 mL denotes the large amount of antibody purified by S-PMA column, demonstrating excellent specificity and purification efficiency of S-PMA column. The OD@A280 value of S-PMA polyclonal antibody after dialysis was 5.56, revealing that the concentrated concentration of the polyclonal antibody obtained was 4.06 mg/mL.

3.4. Characterization of EuNP

The morphology of the EuNP observed using transmission electron microscopy (TEM) is depicted in Fig. 5. It reveals a homogeneous sphere structure with an approximate size of 101 ± 3 nm, consistent with findings in previous papers [42,43]. Additionally, TEM images show polystyrene shell structures with an approximate thickness of 15 nm. The incorporation of europium chelates into polystyrene shells is aimed at enriching the fluorescent signal and enhancing resistance to the quenching effects of the matrix. Similar core-shell nanocomposites have been reported using this approach, including Fe_2O_3@polystyrene [44], SiO_2@polystyrene [45] and encapsulated quantum dots [46]. Fluorescent analysis confirmed the large Stokes shift (~273 nm) with a narrow emission waveband (peak at ~617 nm) and a wide excitation waveband (peak at ~344 nm) (Fig. 6), indicating reduced background noise and higher achievable sensitivity in bioimaging settings [47].

3.5. Optimization of the preparation conditions

Several factors influencing LFIA performance were investigated, as illustrated in Fig. 7. This study primarily investigated four factors: hapten-BSA conjugate concentration, EuNP-Abs concentration, reaction time and buffer pH. Previous studies have demonstrated that the ratio of the fluorescence intensity between the test line and control line (T/C ratio) on the test strip, measured simultaneously, can compensate for background factors [48]. Therefore, the T/C ratio was utilized to determine the results in both previous studies and our current research

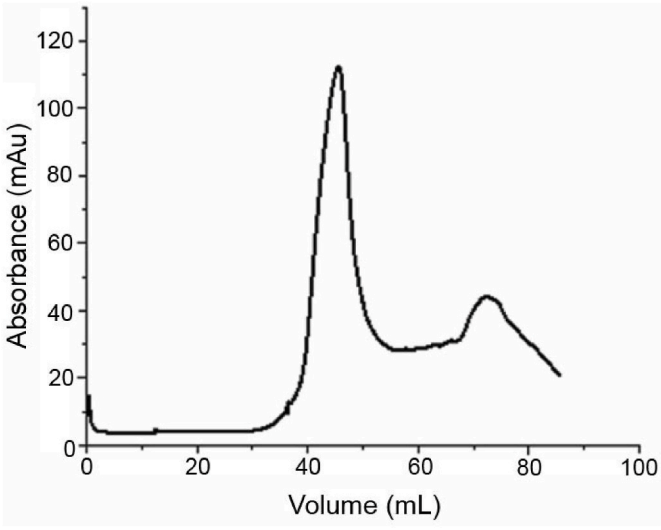

Fig. 3. The chromatogram of purified synthetic hapten-BSA conjugate at an absorption wavelength of 280 nm.

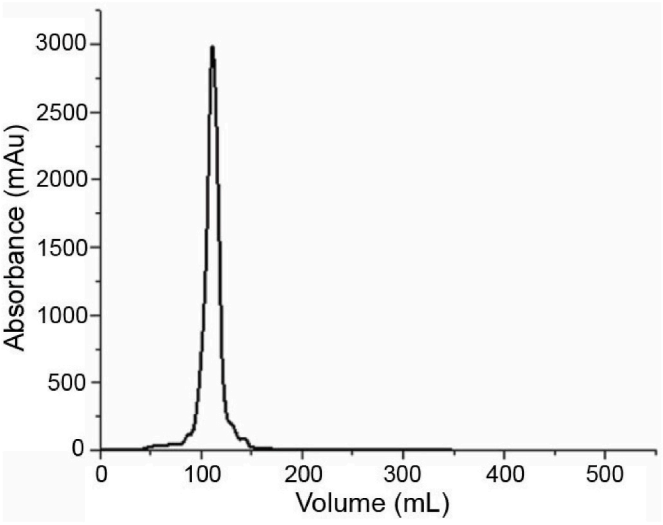

Fig. 4. The FPLC curve of S-PMA after purification at an absorption wavelength of 280 nm.

[49,50]. As shown in Fig. 7 (A), the T/C ratio significantly increased with the escalating dispensing hapten-BSA conjugate concentration from 0.2 to 1.0 mg/mL and when hapten-BSA conjugate concentration reached 1.0 mg/mL, the T/C ratio stabilized and was maintained to 1.4 mg/mL. Moreover, Fig. 7 (B) demonstrates that the T/C ratio increased with the rise in EuNP-Abs concentration on conjugate pads, reaching its maximum at an EuNP-Abs concentration of 1.0 μL/cm. Reaction time is also proved to be a critical factor affecting LFIA performance [51]. The T/C ratio gradually reached maximum around 15 min, indicating that the optimal readout time is 15 min (Fig. 7 (C)). To achieve the highest immunoreaction efficiency, the pH of detection buffer was optimized, as shown in Fig. 7 (D). Buffers with pH ranging from 5 to 10 were prepared. The T/C ratio was highest at a buffer pH of 8, indicating the optimal buffer pH for immunoreaction is 8. Subsequent studies were all conducted under optimal conditions.

3.6. Detection performance

The proposed LFIA approach was applied to determine S-PMA levels in the spiked buffer under the optimal conditions described above. Fig. 8A shows that LFIA strips images with spiked buffer of varying S-PMA levels. Due to the competitive binding method, the higher the S-PMA concentration in the sample, the weaker the fluorescence signal on the test line of the test strip. In Fig. 8B, the calibration curve shows the relationship between the T/C ratio of strips and the S-PMA concentrations of spiked buffer. As the concentration of S-PMA increases, a gradual attenuation of red fluorescence signal becomes evident under a UV (365 nm) lamp. This observation aligns the detection mechanism of competitive immunoassay. Quantitative measurement of the fluorescent signal from the test lines confirmed a reverse correlation. The linear range of the detection for S-PMA was from 0.25 to 30 ng/mL with a linear relationship of $Y = -0.441 \log (C_{S\text{-}PMA}) + 0.659$ where Y is the T/C ratio and the $C_{S\text{-}PMA}$ is the concentration of S-PMA. The coefficient of determination (R^2) is 0.980. The calculated limit of detection (LOD) was determined to be 0.32 ng/mL, based on the three times signal-to-noise ratio standard. Previous study has shown that the concentration of S-PMA in human urine ranges from 0.934 to 14.0 ng/mL, which indicates that the LFIA introduced in this study can effectively detect S-PMA levels in human urine [21]. The American Conference of Governmental Industrial Hygienists recommends a biological exposure index for S-PMA of 25 μg/g creatinine, while European Chemicals Agency sets a biological limit values for S-PMA at 2 μg S-PMA/g creatinine [52]. Additional, the concentration of creatinine in human urine typically ranges from 80

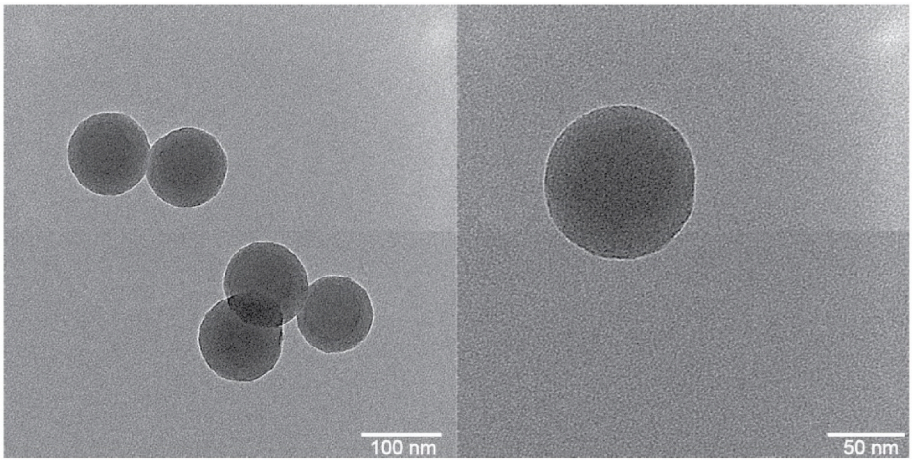

Fig. 5. Transmission electron microscopy (TEM) images of EuNPs.

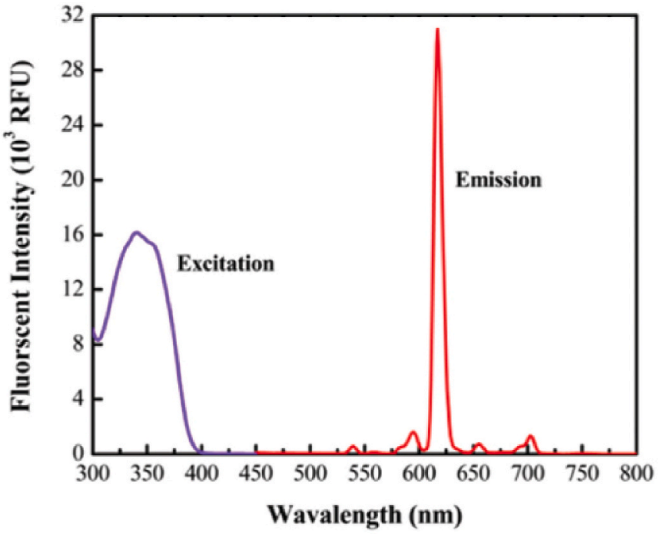

Fig. 6. Fluorescence property of EuNPs.

to 200 μg/dL [53]. The LOD of LFIA is significantly lower than the above standards, which demonstrates the feasibility of its practical application. Certain urinary metabolites with structural similarities to PMA may interfere with its detection, potentially impacting data interpretation [24,55]. However, Aston et al. [24], reported that the PMA immunoassays are not affected by benzylmercapturic acid, a urinary metabolite of toluene. This finding is particularly relevant given the frequent co-exposure to benzene and toluene. Additionally, hippuric acid, a non-specific metabolite of toluene with low structural similarity to PMA, did not cause significant interference in PMA immunoassays.

The detection range and LOD of various approaches for detecting S-PMA are shown in Table 1. Previous studies indicate that conventional detection approaches such as LC-MS, LC-MS/MS GC-MS and HPLC are widely used for S-PMA detection [13,54,55]. However, the extraction and purification process prior to detection make these approaches time-consuming and the expensive equipment makes detection costly [56–58]. At the same time, many novel detection approaches, such as fluorescence quench and surface enhanced Raman spectroscopy (SERS), have been developed, but they struggle to match the detection accuracy of conventional approaches [26,59]. In comparison, the LFIA in this work reduced the LOD of S-PMA to levels comparable with conventional approaches, while greatly simplifying the operation steps, achieving rapid, cheap and accurate detection of S-PMA.

3.7. Stability test

Product stability is a key indicator of LFIA performance andthe stability test results are shown in Fig. 9. According to the accelerated aging calculator, aging at 50 °C for 7 weeks is functionally equivalent to one year at room temperature. The accelerated aging method is based on the Arrhenius reaction rate function, which assumes that a 10 °C increase in temperature will cause the reaction rate to double. The results indicate that LFIA performance remained relatively stable over a nine-week period at 50 °C. The inhibition rate (B/B_0) is often used to reflect the detection performance of LFIA [61,62]. Here, the T/C ratio of the S-PMA spiked samples was defined as B, and the T/C ratio of the control sample is defined as B_0 [63]. In this study, B/B_0 is used to assess the stability of LFIA detection. The result of B/B_0 can not only demonstrate the LFIA's ability to detect different levels of S-PMA, but also reflect the proportional relationship between samples with different S-PMA levels and the control sample. In stability testing, LFIA maintained performance above 90 % after nine weeks of aging. Specifically, when measuring S-PMA levels at 0.5 ng/mL, the LFIA's detection performance decreased by only 6.9 % after nine weeks of storage, demonstrating stable performance. Furthermore, when testing various concentrations of S-PMA, LFIA produced relatively stable results at different aging times. These fundings indicate that LFIA can maintain relatively stable detection performance during the aging test period. In summary, the aging test results show that LFIA can be stored at room temperature for one year while maintaining reliable analytical detection performance. Additionally, the average relative standard deviation (RSD) of the test data from ten LFIA test strips in the same batch is 2.54 ± 0.763 %, while RSD of LFIA test strips across three batches is 2.40 ± 1.28 %. The intra- and inter-batch differences are well within the acceptable range for a biological assay (limit of 20 %) [64].

4. Conclusion

In conclusion, this study presents a novel LFIA-based method for the sensitive and quantitative detection of urinary S-PMA, offering a rapid and effective tool for assessing short-term wood smoke exposure in humans. By eliminating the need for sample pretreatment steps such as extraction, purification, and enzymatic or acid hydrolysis required by conventional methods, this approach significantly reduces assay time while maintaining high sensitivity. The use of EuNPs, renowned for their large Stokes shift, high fluorescence brightness, and stability, as antibody-conjugated detector probes enables ultrasensitive detection of S-PMA, achieving a detection limit of 0.32 ng/mL and a broad detection range of 0.10–30 ng/mL. The developed EuNP-based LFIA strips also demonstrated excellent stability, retaining over 90 % of their detection

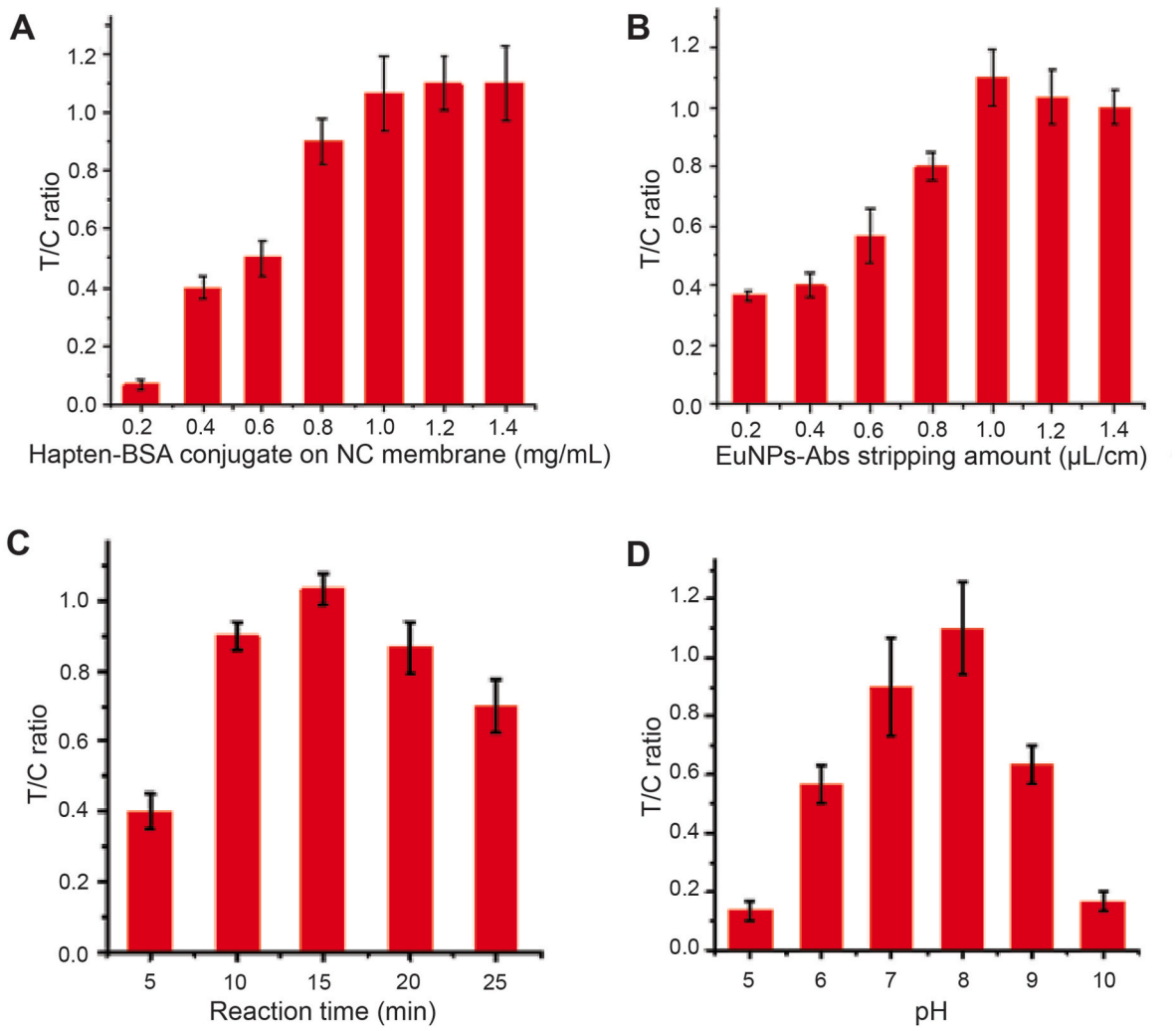

Fig. 7. The optimization of the detection conditions of LFIA. (A) Effect of different concentrations of hapten-BSA conjugate on NC membrane. (B) Effect of different amounts of EuNP-Abs on the conjugate pad. (C) Effect of reaction time of immunoreaction. (D) Effect of pH of detection buffer.

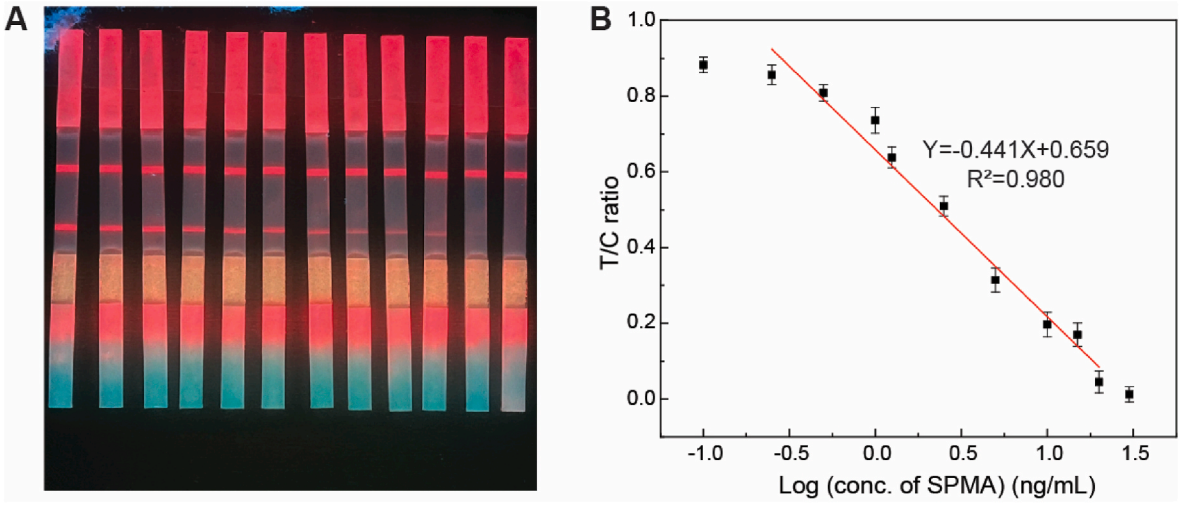

Fig. 8. **(A)** Lateral flow immunoassays images of spiked buffer with different S-PMA levels. The S-PMA levels in the spiked buffer, from left to right, are 0, 0.1, 0.25, 0.5, 1, 1.25, 2.5, 5, 10, 15, 20, 30 ng/mL. **(B)** Calibration curve of T/C ratio of strips versus concentrations of spiked buffer. T/C ratio: fluorescent intensity of the test line to the control line ratio.

Table 1
Performance of various approaches for the detection of S-PMA.

Approach	LOD	Detection range	Ref.
LC-MS	0.5 ng/mL (LOQ)[a]	/	[13]
LC-MS/MS	50 ng/mL	0.5–500 ng/mL	[54]
	0.6 ng/mL[b]	/	[21]
	0.15 ng/mL		
	0.08 ng/mL		
	0.024 ng/mL		
	0.2 ng/mL		
HPLC-UV/Vis	8 ng/mL	30–1000 ng/mL	[55]
HPLC/AC/DBMNs[c]	10 ng/mL	30–1000 ng/mL	[60]
Luminescent probe	3.0×10^{-8} M	3.70–180 μM	[59]
SIPS[d]/SERS	1.06 ppb	0–5 ppm	[26]
GC-MS	0.1 ng/mL	/	[56]
LFIA	0.32 ng/mL	0.25–30 ng/mL	This work

[a] Only limit of quantitation (LOQ) was reported in this study.
[b] Five LC-MS parameters were set for the detection of S-PMA, and thus five different LODs were reported in this study.
[c] AC/DBMNs refers to activated carbon/diatomite-based magnetic nanocomposites.
[d] SIPS refers to salt-induced phase separation.

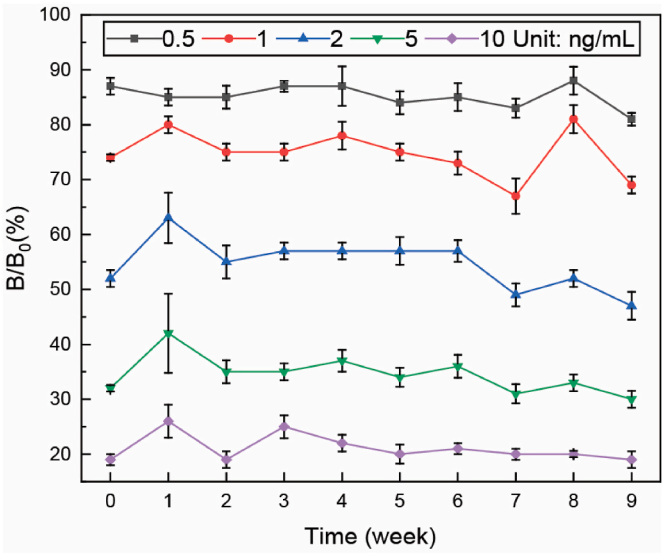

Fig. 9. B/B_0 results of LFIA for S-PMA of different levels in stability test. S-PMA levels in samples: Black 0.5 ng/mL; Red 1 ng/mL; Blue 2 ng/mL; Green 5 ng/mL; Purple 10 ng/mL. (For interpretation of the references to colour in this figure legend, the reader is referred to the Web version of this article.)

performance after one year. This low-cost, user-friendly diagnostic tool complements blood-based diagnostics, providing a comprehensive and practical option for exposure assessment. Furthermore, this work highlights the potential of LFIA technology in advancing the development of rapid, precise, cost-effective, and portable detection devices for biomonitoring applications.

CRediT authorship contribution statement

Yonghao Fu: Writing – original draft, Methodology, Investigation, Data curation, Conceptualization. **Yang Song:** Writing – original draft, Methodology, Investigation, Data curation, Conceptualization. **Zhansen Yang:** Writing – original draft, Investigation, Data curation. **Xiaofan Ruan:** Writing – original draft, Investigation, Conceptualization. **Yuehe Lin:** Writing – review & editing, Supervision, Methodology, Conceptualization. **Dan Du:** Writing – review & editing, Supervision, Methodology, Funding acquisition, Conceptualization.

Declaration of competing interest

The authors declare that they have no known competing financial interests or personal relationships that could have appeared to influence the work reported in this paper.

Acknowledgments

This study was supported by the Centers for Disease Control and Prevention/National Institute for Occupational Safety and Health, CDC/NIOSH) grant (1 R01OH012579-01-00).

Data availability

No data was used for the research described in the article.

References

[1] J.C. Liu, L.J. Mickley, M.P. Sulprizio, F. Dominici, X. Yue, K. Ebisu, G.B. Anderson, R.F.A. Khan, M.A. Bravo, M.L. Bell, Particulate air pollution from wildfires in the Western US under climate change, Clim. Change 138 (3) (2016) 655–666, https://doi.org/10.1007/s10584-016-1762-6.
[2] D.A. Jaffe, S.M. O'Neill, N.K. Larkin, A.L. Holder, D.L. Peterson, J.E. Halofsky, A. G. Rappold, Wildfire and prescribed burning impacts on air quality in the United States, J. Air Waste Manag. Assoc. 70 (6) (2020) 583–615, https://doi.org/10.1080/10962247.2020.1749731.
[3] O. Adetona, C.D. Simpson, Z. Li, A. Sjodin, A.M. Calafat, L.P. Naeher, Hydroxylated polycyclic aromatic hydrocarbons as biomarkers of exposure to wood smoke in wildland firefighters, J. Expo. Sci. Environ. Epidemiol. 27 (1) (2017) 78–83, https://doi.org/10.1038/jes.2015.75.
[4] C.M. Williamson-Reisdorph, K.G. Tiemessen, K. Christison, S. Gurney, D. Richmond, K. Wood, T.S. Quindry, C.L. Dumke, J.C. Quindry, Cardiovascular and blood oxidative stress responses to exercise and acute woodsmoke exposure in recreationally active individuals, Wilderness Environ. Med. 33 (1) (2022) 17–24, https://doi.org/10.1016/j.wem.2021.10.002.
[5] M. Valière, P. Petit, R. Persoons, C. Demeilliers, A. Maître, Consistency between air and biological monitoring for assessing polycyclic aromatic hydrocarbon exposure and cancer risk of workers, Environ. Res. 207 (2022) 112268, https://doi.org/10.1016/j.envres.2021.112268.
[6] L.P. Naeher, M. Brauer, M. Lipsett, J.T. Zelikoff, C.D. Simpson, J.Q. Koenig, K. R. Smith, Woodsmoke health effects: a review, Inhal. Toxicol. 19 (1) (2007) 67–106, https://doi.org/10.1080/08958370600985875.
[7] C.D. Simpson, L.P. Naeher, Biological monitoring of wood-smoke exposure, Inhal. Toxicol. 22 (2) (2010) 99–103, https://doi.org/10.3109/08958370903008862.
[8] B. Barros, M. Oliveira, S. Morais, Biomonitoring of firefighting forces: a review on biomarkers of exposure to health-relevant pollutants released from fires, J. Toxicol. Environ. Health, Part A B 26 (3) (2023) 127–171, https://doi.org/10.1080/10937404.2023.2172119.
[9] S.M. Arnold, J. Angerer, P.J. Boogaard, M.F. Hughes, R.B. O'Lone, S.H. Robison, A. Robert Schnatter, The use of biomonitoring data in exposure and human health risk assessment: benzene case study, Crit. Rev. Toxicol. 43 (2) (2013) 119–153, https://doi.org/10.3109/10408444.2012.756455.
[10] P.J. Boogaard, N.J. van Sittert, Suitability of S-phenyl mercapturic acid and trans-trans-muconic acid as biomarkers for exposure to low concentrations of benzene, Environ. Health Perspect. 104 (suppl 6) (1996) 1151–1157, https://doi.org/10.1289/ehp.961041151.
[11] A.A. Melikian, R. O'Connor, A.K. Prahalad, P. Hu, H. Li, M. Kagan, S. Thompson, Determination of the urinary benzene metabolites S-phenylmercapturic acid and trans, trans-muconic acid by liquid chromatography-tandem mass spectrometry, Carcinogenesis 20 (4) (1999) 719–726, https://doi.org/10.1093/carcin/20.4.719.
[12] L.-C. Lin, W.-J. Chen, Y.-M. Chiung, T.-S. Shih, P.-C. Liao, Association between GST genetic polymorphism and dose-related production of urinary benzene metabolite markers, trans, trans-muconic acid and S-phenylmercapturic acid, Cancer Epidemiol. Biomark. Prev. 17 (6) (2008) 1460–1469, https://doi.org/10.1158/1055-9965.
[13] C. Rosting, R. Olsen, Biomonitoring of the benzene metabolite s-phenylmercapturic acid and the toluene metabolite s-benzylmercapturic acid in urine from firefighters, Toxicol. Lett. 329 (2020) 20–25, https://doi.org/10.1016/j.toxlet.2020.04.018.
[14] G. Tranfo, D. Pigini, E. Paci, L. Bauleo, F. Forastiere, C. Ancona, Biomonitoring of urinary benzene metabolite SPMA in the general population in Central Italy, Toxics 6 (3) (2018), https://doi.org/10.3390/toxics6030037.
[15] P. Lovreglio, M.N. D'Errico, S. Fustinoni, I. Drago, A. Barbieri, L. Sabatini, M. Carrieri, P. Apostoli, L. Soleo, Biomarkers of internal dose for the assessment of environmental exposure to benzene, J. Environ. Monit. 13 (10) (2011) 2921–2928, https://doi.org/10.1039/C1EM10512D.
[16] L.L. Aylward, C.R. Kirman, R. Schoeny, C.J. Portier, S.M. Hays, Evaluation of biomonitoring data from the CDC national exposure report in a risk assessment context: perspectives across chemicals, Environ. Health Perspect. 121 (3) (2013) 287–294, https://doi.org/10.1289/ehp.1205740.

[17] K. Vorkamp, A. Castaño, J.-P. Antignac, L.D. Boada, E. Cequier, A. Covaci, M. Esteban López, L.S. Haug, M. Kasper-Sonnenberg, H.M. Koch, O. Pérez Luzardo, A. Osīte, L. Rambaud, M.-T. Pinorini, G. Sabbioni, C. Thomsen, Biomarkers, matrices and analytical methods targeting human exposure to chemicals selected for a European human biomonitoring initiative, Environ. Int. 146 (2021) 106082, https://doi.org/10.1016/j.envint.2020.106082.
[18] C. Chen, Y. Fu, S.S. Sparks, Z. Lyu, A. Pradhan, S. Ding, N. Boddeti, Y. Liu, Y. Lin, D. Du, K. Qiu, 3D-Printed flexible microfluidic health monitor for in situ sweat analysis and biomarker detection, ACS Sens. (2024), https://doi.org/10.1021/acssensors.4c00528.
[19] J. Angerer, U. Ewers, M. Wilhelm, Human biomonitoring: state of the art, Int. J. Hyg Environ. Health 210 (3) (2007) 201–228, https://doi.org/10.1016/j.ijheh.2007.01.024.
[20] C. Judy, M. Thit Aarøe, J. Anke, E.K. Lisbeth, Major national human biomonitoring programs in chemical exposure assessment, AIMS Environmental Science 2 (3) (2015) 782–802, https://doi.org/10.3934/environsci.2015.3.782.
[21] D.S. Tevis, A. Willmore, D. Bhandari, B. Bowman, C. Biren, B.M. Kenwood, P. Jacob, J. Liu, K. Bello, S.S. Hecht, S.G. Carmella, M. Chen, E. Gaudreau, J.-F. Bienvenu, B.C. Blount, V.R. De Jesús, Large differences in urinary benzene metabolite S-phenylmercapturic acid quantitation: a comparison of five LC–MS-MS methods, J. Anal. Toxicol. 45 (7) (2021) 657–665, https://doi.org/10.1093/jat/bkaa137.
[22] M.P.R. Mendes, J.N. Silveira, L.C. Andre, An efficient analytical method for determination of S-phenylmercapturic acid in urine by HPLC fluorimetric detector to assessing benzene exposure, J. Chromatogr. B 1063 (2017) 136–140, https://doi.org/10.1016/j.jchromb.2017.07.039.
[23] G. Marrubini, S. Dugheri, M. Pacenti, T. Coccini, G. Arcangeli, V. Cupelli, L. Manzo, Determination of S-phenylmercapturic acid by GC-MS and ELISA: a comparison of the two methods, Biomarkers 10 (4) (2005) 238–251, https://doi.org/10.1080/13547500500218757.
[24] J.P. Aston, R.L. Ball, J.E. Pople, K. Jones, J. Cocker, Development and validation of a competitive immunoassay for urinary S-phenylmercapturic acid and its application in benzene biological monitoring, Biomarkers 7 (2) (2002) 103–112, https://doi.org/10.1080/13547500110099663.
[25] V. Yusa, M. Millet, C. Coscolla, M. Roca, Analytical methods for human biomonitoring of pesticides. A review, Anal. Chim. Acta 891 (2015) 15–31, https://doi.org/10.1016/j.aca.2015.05.032.
[26] H. Wei, W. Zou, R. Feng, L. Liu, M. Zhang, X. Meng, W. Chen, Q. Jia, C. Wang, Point-of-Care testing of benzene metabolite S-phenylmercapturic acid using salt-induced phase separation combined with nanoparticle-based surface-enhanced Raman spectroscopy, ACS Appl. Nano Mater. 7 (14) (2024) 16237–16244, https://doi.org/10.1021/acsanm.4c02165.
[27] M. Ding, S. Ding, D. Du, X. Wang, X. Hu, P. Guan, Z. Lyu, Y. Lin, Recent advances in electrochemical biosensors for the detection of Aβ42, a biomarker for Alzheimer disease diagnosis, TrAC, Trends Anal. Chem. 164 (2023) 117087, https://doi.org/10.1016/j.trac.2023.117087.
[28] X. Ruan, Y. Wang, N. Cheng, X. Niu, Y.-C. Chang, L. Li, D. Du, Y. Lin, Emerging applications of additive manufacturing in biosensors and bioanalytical devices, Advanced Materials Technologies 5 (7) (2020) 2000171, https://doi.org/10.1002/admt.202000171.
[29] V. Naresh, N. Lee, A review on biosensors and recent development of nanostructured materials-enabled biosensors, Sensors 21 (4) (2021), https://doi.org/10.3390/s21041109.
[30] J. Kirsch, C. Siltanen, Q. Zhou, A. Revzin, A. Simonian, Biosensor technology: recent advances in threat agent detection and medicine, Chem. Soc. Rev. 42 (22) (2013) 8733–8768, https://doi.org/10.1039/C3CS60141B.
[31] F.S. Felix, L. Angnes, Electrochemical immunosensors – a powerful tool for analytical applications, Biosens. Bioelectron. 102 (2018) 470–478, https://doi.org/10.1016/j.bios.2017.11.029.
[32] Katarzyna M. Koczula, A. Gallotta, Lateral flow assays, Essays Biochem. 60 (1) (2016) 111–120, https://doi.org/10.1042/EBC20150012.
[33] E.B. Bahadır, M.K. Sezgintürk, Lateral flow assays: principles, designs and labels, TrAC, Trends Anal. Chem. 82 (2016) 286–306, https://doi.org/10.1016/j.trac.2016.06.006.
[34] M. Sajid, A.-N. Kawde, M. Daud, Designs, formats and applications of lateral flow assay: a literature review, J. Saudi Chem. Soc. 19 (6) (2015) 689–705, https://doi.org/10.1016/j.jscs.2014.09.001.
[35] Z. Lyu, S. Ding, P. Tieu, L. Fang, X. Li, T. Li, X. Pan, M.H. Engelhard, X. Ruan, D. Du, S. Li, Y. Lin, Single-atomic site catalyst enhanced lateral flow immunoassay for point-of-care detection of herbicide, Research 2022, http://doi.org/10.34133/2022/9823290, 2022.
[36] X. Ruan, Y. Wang, E.Y. Kwon, L. Wang, N. Cheng, X. Niu, S. Ding, B.J. Van Wie, Y. Lin, D. Du, Nanomaterial-enhanced 3D-printed sensor platform for simultaneous detection of atrazine and acetochlor, Biosens. Bioelectron. 184 (2021) 113238, https://doi.org/10.1016/j.bios.2021.113238.
[37] X. Ruan, V. Hulubei, Y. Wang, Q. Shi, N. Cheng, L. Wang, Z. Lyu, W.C. Davis, J. N. Smith, Y. Lin, D. Du, Au@PtPd enhanced immunoassay with 3D printed smartphone device for quantification of diaminochlorotriazine (DACT), the major atrazine biomarker, Biosens. Bioelectron. 208 (2022) 114190, https://doi.org/10.1016/j.bios.2022.114190.
[38] N. Cheng, Q. Shi, C. Zhu, S. Li, Y. Lin, D. Du, Pt–Ni(OH)2 nanosheets amplified two-way lateral flow immunoassays with smartphone readout for quantification of pesticides, Biosens. Bioelectron. 142 (2019) 111498, https://doi.org/10.1016/j.bios.2019.111498.
[39] N. Cheng, Y. Song, M.M.A. Zeinhom, Y.-C. Chang, L. Sheng, H. Li, D. Du, L. Li, M.-J. Zhu, Y. Luo, W. Xu, Y. Lin, Nanozyme-mediated dual immunoassay integrated with smartphone for use in simultaneous detection of pathogens, ACS Appl. Mater. Interfaces 9 (46) (2017) 40671–40680, https://doi.org/10.1021/acsami.7b12734.
[40] Y. Song, X. Cai, G. Ostermeyer, J. Yu, D. Du, Y. Lin, Self-assembling allochroic nanocatalyst for improving nanozyme-based immunochromatographic assays, ACS Sens. 6 (1) (2021) 220–228, https://doi.org/10.1021/acssensors.0c02148.
[41] J.M. Fowler, D.K.Y. Wong, H.B. Halsall, W.R. Heineman, Chapter 5 - recent developments in electrochemical immunoassays and immunosensors, in: X. Zhang, H. Ju, J. Wang (Eds.), Electrochemical Sensors, Biosensors and Their Biomedical Applications, Academic Press, San Diego, 2008, pp. 115–143, https://doi.org/10.1016/B978-012373738-0.50007-6.
[42] T. Soukka, H. Härmä, J. Paukkunen, T. Lövgren, Utilization of kinetically enhanced monovalent binding affinity by immunoassays based on multivalent nanoparticle-antibody bioconjugates, Anal. Chem. 73 (10) (2001) 2254–2260, https://doi.org/10.1021/ac001287l.
[43] L. Kokko, T. Lövgren, T. Soukka, Europium(III)-chelates embedded in nanoparticles are protected from interfering compounds present in assay media, Anal. Chim. Acta 585 (1) (2007) 17–23, https://doi.org/10.1016/j.aca.2006.12.006.
[44] Y. Wang, X. Teng, J.-S. Wang, H. Yang, Solvent-free atom transfer radical polymerization in the synthesis of Fe_2O_3@Polystyrene Core−Shell nanoparticles, Nano Lett. 3 (6) (2003) 789–793, https://doi.org/10.1021/nl034211o.
[45] S.-W. Zhang, S.-X. Zhou, Y.-M. Weng, L.-M. Wu, Synthesis of SiO2/polystyrene nanocomposite particles via miniemulsion polymerization, Langmuir 21 (6) (2005) 2124–2128, https://doi.org/10.1021/la047652b.
[46] H. Kloust, C. Schmidtke, J.-P. Merkl, A. Feld, T. Schotten, U.E.A. Fittschen, M. Gehring, J. Ostermann, E. Pöselt, H. Weller, Poly(ethylene oxide) and polystyrene encapsulated quantum dots: highly fluorescent, functionalizable, and ultrastable in aqueous media, J. Phys. Chem. C 117 (44) (2013) 23244–23250, https://doi.org/10.1021/jp4045836.
[47] T.-B. Ren, W. Xu, W. Zhang, X.-X. Zhang, Z.-Y. Wang, Z. Xiang, L. Yuan, X.-B. Zhang, A general method to increase Stokes shift by introducing alternating vibronic structures, J. Am. Chem. Soc. 140 (24) (2018) 7716–7722, https://doi.org/10.1021/jacs.8b04404.
[48] C. Wang, F. Hou, Y. Ma, Simultaneous quantitative detection of multiple tumor markers with a rapid and sensitive multicolor quantum dots based immunochromatographic test strip, Biosens. Bioelectron. 68 (2015) 156–162, https://doi.org/10.1016/j.bios.2014.12.051.
[49] Q. Yang, X. Gong, T. Song, J. Yang, S. Zhu, Y. Li, Y. Cui, Y. Li, B. Zhang, J. Chang, Quantum dot-based immunochromatography test strip for rapid, quantitative and sensitive detection of alpha fetoprotein, Biosens. Bioelectron. 30 (1) (2011) 145–150, https://doi.org/10.1016/j.bios.2011.09.002.
[50] E.G. Rey, D. O'Dell, S. Mehta, D. Erickson, Mitigating the hook effect in lateral flow sandwich immunoassays using real-time reaction kinetics, Anal. Chem. 89 (9) (2017) 5095–5100, https://doi.org/10.1021/acs.analchem.7b00638.
[51] M. Shen, Y. Chen, Y. Zhu, M. Zhao, Y. Xu, Enhancing the sensitivity of lateral flow immunoassay by centrifugation-assisted flow control, Anal. Chem. 91 (7) (2019) 4814–4820, https://doi.org/10.1021/acs.analchem.9b00421.
[52] J. Morton, C. Sams, E. Leese, F. Garner, S. Iqbal, K. Jones, Biological monitoring: evidence for reductions in occupational exposure and risk, Frontiers in Toxicology 4 (2022), https://doi.org/10.3389/ftox.2022.836567.
[53] B. Barr Dana, C. Wilder Lynn, P. Caudill Samuel, J. Gonzalez Amanda, L. Needham Lance, L. Pirkle James, Urinary creatinine concentrations in the U.S. Population: implications for urinary biologic monitoring measurements, Environ. Health Perspect. 113 (2) (2005) 192–200, https://doi.org/10.1289/ehp.7337.
[54] A.P. Gomes, E. Barbosa, A.L.A.d. Santos, L.F. Lizot, E. Sauer, S.C. Garcia, R. Linden, M.V. Antunes, M.F. Charao, A simple and sensitive LC-MS/MS method for the determination of S-phenylmercapturic acid in human urine, Quim. Nova 44 (2021) 334–340, https://doi.org/10.21577/0100-4042.20170651.
[55] H. Ye, J. Shao, Y. Shi, S. Tan, K. Su, L. Zhang, X. Shan, Magnetic molecularly imprinted polymers for extraction of S-phenylmercapturic acid from urine samples followed by high-performance liquid chromatography, J. Mol. Recogn. 34 (11) (2021) e2930, https://doi.org/10.1002/jmr.2930.
[56] S. Dugheri, N. Mucci, G. Cappelli, A. Bonari, M. Campagna, G. Arcangeli, G. Bartolucci, New fully automated gas chromatographic analysis of urinary S-phenylmercapturic acid in isotopic dilution using negative chemical ionization with isobutane as reagent gas, J. Mass Spectrom. 55 (7) (2020) e4481, https://doi.org/10.1002/jms.4481.
[57] B.G. Keevil, LC-MS/MS the first 20 years: a personal view, Ann. Clin. Biochem. 59 (1) (2022) 3–6, https://doi.org/10.1177/00045632211040059.
[58] A. Nasiri, R. Jahani, S. Mokhtari, H. Yazdanpanah, B. Daraei, M. Faizi, F. Kobarfard, Overview, consequences, and strategies for overcoming matrix effects in LC-MS analysis: a critical review, Analyst 146 (20) (2021) 6049–6063, https://doi.org/10.1039/D1AN01047F.
[59] W. Li, D. Li, Y. Yang, S. Su, S. Qie, Y. Jia, M. Hu, Identification of *S*-phenylmercapturic acid using heterometallic Zn–Eu MOF as a fluorescence sensor, J. Mol. Struct. 1321 (2025) 139974, https://doi.org/10.1016/j.molstruc.2024.139974.
[60] X. Shan, S. Tan, Y. Shi, J. Shao, K. Su, L. Zhang, H. Feng, H. Ye, Activated carbon/diatomite-based magnetic nanocomposites for magnetic solid-phase extraction of S-phenylmercapturic acid from human urine, Biomed. Chromatogr. 34 (7) (2020) e4834, https://doi.org/10.1002/bmc.4834.
[61] G. Tan, Y. Zhao, M. Wang, X. Chen, B. Wang, Q.X. Li, Ultrasensitive quantitation of imidacloprid in vegetables by colloidal gold and time-resolved fluorescent nanobead traced lateral flow immunoassays, Food Chem. 311 (2020) 126055, https://doi.org/10.1016/j.foodchem.2019.126055.
[62] J. Wang, Q. Wang, Y. Zheng, T. Peng, K. Yao, S. Xie, X. Zhang, X. Xia, J. Li, H. Jiang, Development of a quantitative fluorescence-based lateral flow

immunoassay for determination of chloramphenicol, thiamphenicol and florfenicol in milk, Food Agric. Immunol. 29 (1) (2018) 56–66, https://doi.org/10.1080/09540105.2017.1359498.

[63] Y. Wu, B. Yu, P. Cui, T. Yu, G. Shi, Z. Shen, Development of a quantum dot–based lateral flow immunoassay with high reaction consistency to total aflatoxins in botanical materials, Anal. Bioanal. Chem. 413 (6) (2021) 1629–1637, https://doi.org/10.1007/s00216-020-03123-4.

[64] A.R. Cardoso, F.T.C. Moreira, R. Fernandes, M.G.F. Sales, Novel and simple electrochemical biosensor monitoring attomolar levels of miRNA-155 in breast cancer, Biosens. Bioelectron. 80 (2016) 621–630, https://doi.org/10.1016/j.snb.2015.02.068.